Test Demonstration of Digital Control of Wing/Store Flutter

E.H. Johnson,* C. Hwang,† W.S. Pi,* D.F. Kesler,‡ and D.S. Joshi*
Northrop Corporation, Hawthorne, California
and
C.A. Harvey§
Honeywell, Inc., Minneapolis, Minnesota

Methods of digital control have been applied to a demonstration of the suppression of wing/store flutter. Digital control laws were developed by applying a modified Jordan canonical transformation to a state variable formulation of a control law synthesized originally for an analog system. A real-time simulation of the components of the control system served to develop the concepts. This was followed by a wind-tunnel demonstration which evaluated the system in detail. The results of the test showed that the performance of the digital controller was comparable to that of analog controllers. Attention during the test was focused on the insertion of adequate antialiasing filters, the effects of sample time, and the compensation for phase lags introduced by the digital control process.

Introduction

IN 1979, flutter suppression techniques were successfully demonstrated in the NASA Langley Research Center's Transonic Dynamics Tunnel using a half-span scale model of the YF-17 (Fig. 1). References 1-3 give the results of that program, which tested a number of control laws developed by various investigators. In the same time frame, an analytical feasibility demonstration on the applicability of adaptive control methods to active flutter suppression was performed.[4] That study naturally presupposed that the controller would be a digital computer instead of the analog circuitry that had been used in all the previous demonstrations. A new program was thus initiated in 1980 that combined these parallel efforts in a program entitled Test Demonstration of Digital Adaptive Control of Wing/Store Flutter. The program was organized in two phases, with the first phase concentrated on the demonstration of digital control and adaptive control emphasized in the second. This paper reports on the digital demonstration, with adaptive aspects mentioned only as they impact on this demonstration.

The use of a digital control system for flutter suppression contrasts with the large number of demonstrations that have been carried out using analog control systems (e.g., Refs. 5 and 6). An exception is a wind-tunnel test program in which digital active flutter suppression on a 1/30 scale B-52 aeroelastic model was demonstrated.[7] In the test, the system performed effectively and demonstrated a 24% improvement in the flutter dynamic pressure.

Because this paper describes a demonstration program, the content emphasizes descriptions of the systems developed and the results obtained during the wind-tunnel entry, with a minimal discussion of the theoretical concepts involved. After briefly describing the wind-tunnel model and the configuration tested, ensuing sections of the paper describe the techniques used to develop the digital control laws, the simulation laboratory assembled for the project, and the wind-tunnel test program. In a final section, the results of the test are commented upon and conclusions and recommendations are offered.

Presented as Paper 82-0645 at the AIAA/ASME/ASCE/AHS 23rd Structures, Structural Dynamics and Materials Conference, New Orleans, La., May 10-12, 1982; submitted May 28, 1982; revision received Jan. 7, 1983.

*Engineering Specialist, Aircraft Division. Member AIAA.
†Manager, Structural Dynamics Research, Aircraft Division. Associate Fellow AIAA.
‡Senior Technical Specialist, Aircraft Division.
§Principal Staff Engineer.

The Flutter Suppression System

The model used in the previous programs and depicted in Fig. 1 was retained for this program. References 1-3 describe the model in some detail; therefore, only a basic description is offered in this paper. The model is a 30% scale half-span model of the YF-17 and is mounted on roll bars which permit rigid-body longitudinal degrees of freedom. The flutter suppression network basically entails feeding back compensated accelerometer (sensors in Fig. 1) outputs to leading- and/or trailing-edge control surfaces. Unique features of the system include a "flutter detector," an electronic device that senses when large amplitude oscillatory responses occur, and a flutter stopper which fires a mass inside the missile of a key configuration through a remotely controlled spring/latch mechanism. When the mass is deployed, the flutter mechanism of the configuration is disrupted.

A specially designed control console serves as the interface to all components of the flutter suppression system. A key component is the SEL 32/55 digital computer which performs the digital control. This computer is a true 32 bit machine with a floating-point processor. Communication with the wind-tunnel model via the control console is performed using 12 bit analog-to-digital and digital-to-analog circuits. Other features of the system include a hydraulic pump to power the actuators, a trim controller which drives the horizontal tail, and various monitoring instruments, including a Hewlett-Packard Fourier analyzer.

The store configuration used for the majority of the demonstration program is the same configuration B that was tested in the programs described in Refs. 1-3. Configuration B features an AIM-7S missile attached to a pylon located at wing station (WS) 60.5. Its wing tip launch rail is empty (see Fig. 1). This configuration is characterized by a violent flutter condition that had been successfully controlled by analog control laws in the previous programs.

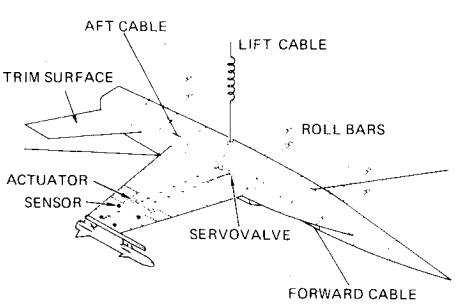

Fig. 1 YF-17 wing/store flutter suppression model, configuration B.

Digitization of Control Laws

As discussed previously, flutter control is effected by operating on the outputs of the accelerometers to create a signal that is fed back to the control surface. The form of this operation, designated the control law, was determined using the synthesis procedure of Ref. 1. (An exception to this procedure is given in Ref. 8, where methods from optimal control theory were applied.) The control law was formulated in the s plane and could therefore be implemented directly by analog devices. This section describes the process required to transform the control law to a form applicable to a digital computer.

Figure 2 shows a representative control law. In the figure, the output of three accelerometers are used in combination to form two basic feedback paths. These two signals are passed through integrators to obtain velocity- and displacement-like responses. Gains determined by the synthesis procedure are applied to each of the four responses, and they are then summed to obtain a single command to the control surface. This signal is conditioned by a string of filters that act to limit the responses at frequencies other than the flutter frequency. The entire control law was implemented on the digital computer. The first step of the implementation was to transform the transfer function relationships of the feedback control law shown in Fig. 2 into a standard first-order form

$$\dot{x}=Fx+Gu \qquad y=Hx \tag{1}$$

where, in this example, u is a vector of the three accelerometer responses, x is a vector of 11 states related to the 11th order control law, and y is a scalar command to the control surface. The F, G, and H matrices are constant coefficient matrices derived from the transfer function of the control law.

In order to minimize the number of arithmetic operations required by Eq. (1), and thereby speed the digital computation, a transformation is performed on the F matrix to make it a block diagonal form with scalar blocks for real eigenvalues and 2×2 blocks for complex pairs of eigenvalues. The coordinate transformation is

$$\bar{x}=Wx \tag{2}$$

where the columns of W^{-1} are eigenvectors corresponding to real eigenvalues, and the real parts and imaginary parts of the eigenvectors corresponding to complex pairs of eigenvalues. That is, suppose the eigenvalues of F are λ_k with λ_k real for $k\le\ell$ and $\lambda_{\ell+2j-1}=-\sigma_j+i\tau_j$, $\lambda_{\ell+2j}=-\sigma_j-i\tau_j$ for $j=1,2,\ldots,(n-\ell)/2$ where n is the dimension of x. Then $W^{-1}=[w_1, w_2,\ldots, w_\ell, \mathrm{Re}w_{\ell+1}, \mathrm{Im}w_{\ell+1}, \ldots, \mathrm{Re}w_{n-1}, \mathrm{Im}w_{n-1}]$ where w_i is the eigenvector corresponding to λ_i. The transformed Eq. (1) is

$$\dot{\bar{x}}=\bar{F}\bar{x}+\bar{G}u \qquad y=\bar{H}\bar{x} \tag{3}$$

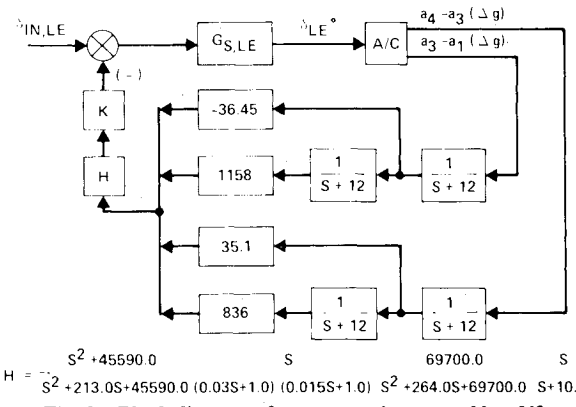

Fig. 2 Block diagram of representative control law N3.

where

$$\bar{F}=WFW^{-1}=\begin{bmatrix} \lambda_1 & & & & & \\ & \ddots & & & & \\ & & \lambda_\ell & & & \\ & & & -\sigma_j & \tau_j & \\ & & & -\tau_j & -\sigma_j & \\ & & & & & \ddots \\ & & & & & & -\sigma_{(n-\ell)/2} & \tau_{(n-\ell)/2} \\ & & & & & & -\tau_{(n-\ell)/2} & -\sigma_{(n-\ell)/2} \end{bmatrix} \tag{4}$$

where

$$\bar{G}=WG, \qquad \bar{H}=HW^{-1}$$

A minor complication is that the integrators of the Fig. 2 control law will give four repeated real eigenvalues of -12. This is avoided by perturbing the values from -12 to make them all unique.

Once the equations are in the form of Eq. (3), the final step is to discretize the continuous equation into the form

$$x_{k+1}=Ax_k+Bu_k \qquad y_{k+1}=Cx_{k+1} \tag{5}$$

where

$$A=e^{\bar{F}T} \qquad B=\bar{G}\int_0^T e^{\bar{F}T}\mathrm{d}t \qquad C=\bar{H} \tag{6}$$

and T is the sample interval and k is the discrete time step indicator. The exponentiations of Eq. (6) are performed using a 36 term series expansion, although for the block diagonal form of $\bar{F}$ an exact calculation could have easily been used.

Figure 3a shows the transfer function of the command to the control surface due to input from the a_4 accelerometer measured across the digital controller. This can be compared with the same measurement made on the analog controller shown in Fig. 3b. It is seen that the two measurements are virtually indistinguishable, with the small differences attributable to different mechanizations of notch filters.

When the control law of Fig. 2 was implemented on a SEL 32/55 computer, it was found that the control computation [i.e., the Eq. (5) calculation] could be performed in 0.8 ms, comfortably faster than the minimum sample interval of 2.5 ms.

Simulation Facility

A key contributor to the success of the program was a real-time simulation of the digital wing/store flutter suppression system. A facility was assembled that included all the hardware that was used in the eventual wind-tunnel demonstration plus additional equipment specific to the simulation. The components of the simulation included the SEL computer, the wind-tunnel model, the flutter console used to interconnect the components, a Fourier analyzer to monitor the system's performance, and a simulation of the airframe's response in the airstream.

The initial simulations were performed on an analog computer, but the required size of the simulation soon outgrew the analog system's capacity, so the airframe simulation was placed on the same SEL digital computer used as the controller.

The equations used in the simulation are based on the aeroelastic equations of motion expressed in the form

$$M\ddot{\xi}+B\dot{\xi}+K\xi+(\rho/\rho_0)A\ddot{\xi}=0 \tag{7}$$

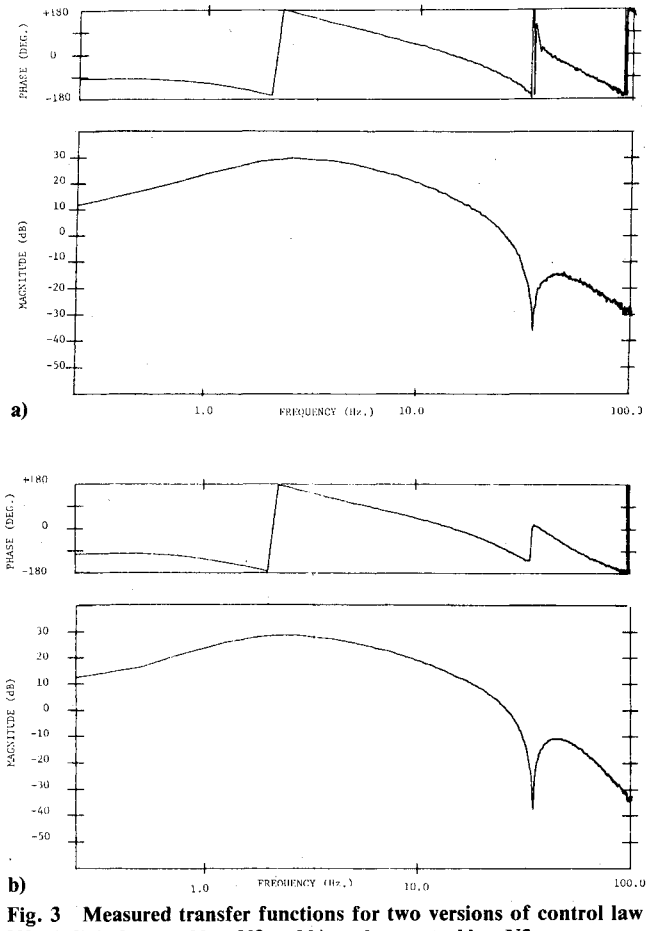

Fig. 3 Measured transfer functions for two versions of control law N3: a) digital control law N3 and b) analog control law N3.

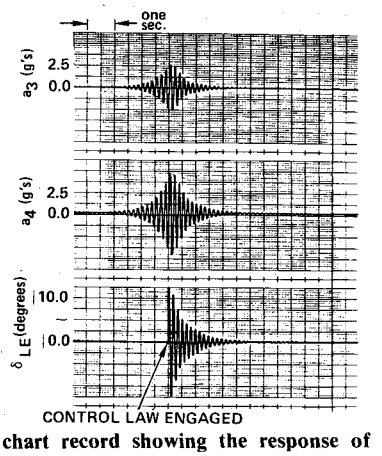

Fig. 4 Strip chart record showing the response of the airframe simulation when the digital control system was engaged.

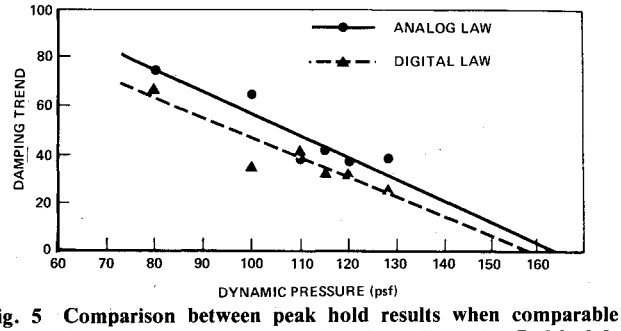

Fig. 5 Comparison between peak hold results when comparable analog and digital control laws are engaged, configuration B, $M=0.8$, N3 control law (TP 86-102).

where ξ represents a vector of modal displacements and M, B, K, and A represent inertia, damping, stiffness, and aerodynamic terms, respectively. The control surface deflections have been included as modal deflections and their associated forces have been included in the matrices.

For the simulation, it was necessary to put the equations in the first-order form of Eq. (1). A complication in reducing Eq. (7) to the form of Eq. (1) is that the aerodynamics are a function of the reduced frequency k. A simple approximation to the complex aerodynamics was made using the equation

$$A_R + iA_I = P_0 + ikP_1 - k^2P_2 \tag{8}$$

where the left sides are the real and imaginary parts of the analytically computed aerodynamic values and are a function of reduced frequency. The P_i terms are constant matrices that correspond to aerodynamic stiffness, damping, and inertia. The P_i matrices are determined by performing a least squares fit solution of the equations over an arbitrarily large range of reduced frequencies. The mechanization of the airframe representation on the digital computer then followed the same process as that discussed for the control law in the previous section.

The actuators of the control surfaces were represented by either including the actual hardware in the simulation or by representing them by an approximating transfer function that had a zero-order numerator and a third-order denominator.

Figure 4 gives a demonstration of the simulation performance by showing the effect of turning the digital controller on to suppress an unstable airframe response. The simulation facility proved indispensable in checking the interconnections among the various hardware components and in debugging the digital software. Ground resonance checks provided assurance that the wind-off behavior of the system was satisfactory.

Wind-Tunnel Test Results

The wind-tunnel entry that tested the concept of digital control of wing/store flutter took place at the NASA Langley Research Center's Transonic Dynamics Tunnel during November 1981. Three weeks were allotted to the entry; the first of these was reserved for the installation and checkout of the model. Significant results from the test include:

1) The damping trends of the digital control laws were comparable to that of their analog counterparts. There was indication of a minor deterioration in the control law performance, in the form of slightly higher control surface activities and model responses when the analog law was changed to a digital law.

2) Variations in the sample time demonstrated that, at a flutter frequency of 6 Hz, adequate control could be obtained with a 10 ms sample time but that the performance deteriorated for longer times.

3) The antialiasing filters installed before the wind-tunnel entry were inadequate. Revised filters developed during the test performed satisfactorily.

4) Compensation for phase lags introduced by the digital control system were necessary in some cases.

The following subsections deal with each of these results.

Digital Control Performance

Configuration B with the N3 control law of Fig. 2 was the primary system tested with the digital controller. Figure 5 compares the peak hold results of the analog and digital implementation of this law. The peak hold device captures the maximum amplitude over a given frequency range. The inverse of the peak amplitude gives a qualitative indication of the damping in the critical mode. The open-loop flutter dynamic pressure is 74 psf. Both the digital and the analog controllers were demonstrated to be stable at dynamic pressures of 70% above this value. The data points in Fig. 5 and the straight line extrapolation of the data, based on a least

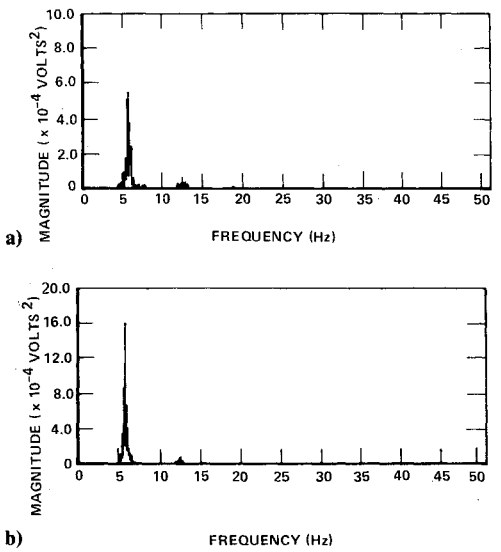

Fig. 6 Comparison of the power spectral density plots of the leading-edge control surface angular displacement, $Q=128$ psf, $M=0.8$: a) analog control law N3 and b) digital control law N3.

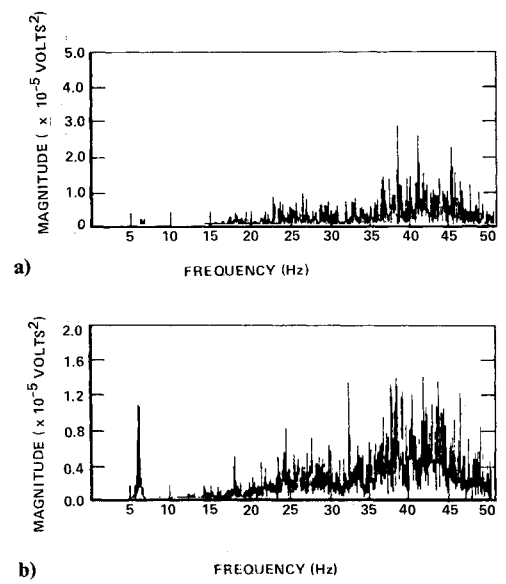

Fig. 7 Comparison of the power spectral density plots of the wing root torsion moment, $Q=128$ psf, $M=0.8$: a) analog control law N3 and b) digital control law N3.

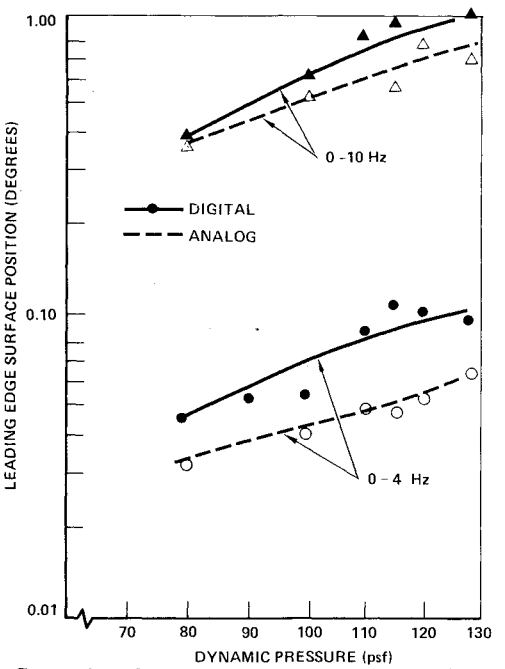

Fig. 8 Comparison between leading-edge control surface activity results for the digital and analog implementations of the N3 control law.

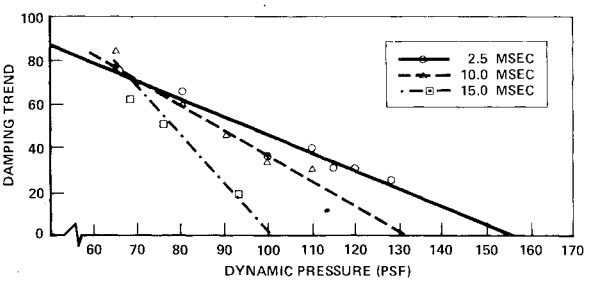

Fig. 9 Comparison among the peak hold results when different sample rates are employed with a digital control law, configuration B, $M=0.8$, N3 control law.

squares fit, show that both laws had ample margin to go to higher dynamic pressures. The damping trend of the digital implementation is slightly lower than that of the analog version.

Other comparisons of the performance of the digital and analog implementations are given in Figs. 6-8. Figure 6 compares power spectral density (PSD) plots of the leading-edge control surface responses of the analog and digital implementations at a similar test condition. It is seen that the digital controller has a larger and sharper peak at the flutter frequency of 6 Hz; a fact observed during the test when the leading-edge deflection was a nearly pure sinusoid when the digital law was used. Figure 7 is another PSD comparison, this time of the torsion strain gage response. The digital controller again shows significantly more response at the flutter frequency, indicating that the analog performance is again superior. (Note that there is a factor of 2.5 difference in the two scales on this plot, exaggerating the difference in the responses.)

Figure 8 compares the rms responses of the leading-edge control surface position. The responses are divided into two frequency ranges to highlight the behavior in the region of the flutter frequency. The digital law is again shown to require more activity, but the difference at the highest dynamic pressure is only about a quarter degree in additional surface motion.

Time Frame Effects

The digital results given in Figs. 5-8 were all obtained at a sample rate of 400 samples/s ($T=2.5$ ms). This was thought to be the fastest rate that would be needed but it is too fast for current aircraft systems. Therefore, it was important to see what effects the sample rate would have on the performance. Figure 9 shows peak hold results at three different sample times. The damping trend shows a constant deterioration as the sample time increases. Figures 10 and 11 show the rms activity for the leading-edge surface and the wing root torsion moment for the three time frames. Over the tested range, the 10 ms results in these figures are very close to the 2.5 ms results, with the 15 ms results showing substantially increased activity in both responses.

There are several factors which contribute to the inferior performance at 15 ms. This corresponds to a 67.0 samples/s rate, which is only slightly above the 50 Hz cutoff of the antialiasing filter. Therefore, significant aliasing occurred at this rate. Another factor is that the 15 ms sample time allows

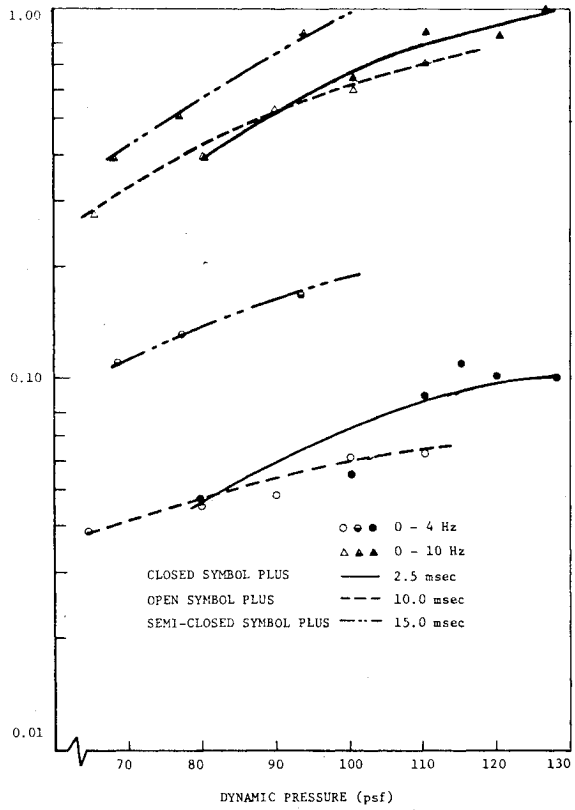

Fig. 10 Comparison among the leading-edge control surface activity results for three different sample rates of the digital implementation of the N3 control law.

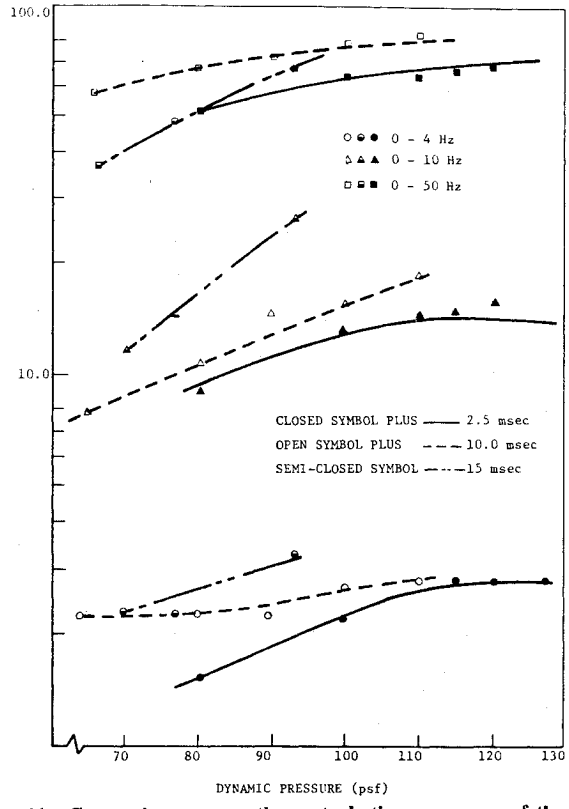

Fig. 11 Comparison among the perturbation responses of the wing root section torsion moment for three different sample rates of the digital implementation of the N3 control law.

for only 11 samples/cycle of the 6 Hz flutter mode. This may be inadequate for high quality control. The sample rate is clearly inadequate in the digital representation of the 34 Hz notch and the 42 Hz low-pass filters of Fig. 2.

Antialiasing Filters

Prior to the tunnel entry, low-pass antialiasing filters that had a 150 Hz cutoff and a second-order rolloff were inserted on the accelerometer outputs before the signals were introduced into the digital computer. At the test site, it was found that the aliasing phenomenon was a more serious problem than had been anticipated and the cutoff frequency was reduced to 50 Hz. This modification was found to be sufficient when the controller was operating at 400 samples/s but was still inadequate when the rate was reduced to 100 samples/s. At the lower rate, it was necessary to install Hewlett-Packard Model 54440A low-pass filters. These filters, at a 50 Hz cutoff, have a sixth-order rolloff and dramatically reduced the amount of aliasing.

Figure 12 provides an indication as to why filtering is necessary. The figure depicts the power spectrum of the a_4 accelerometer response at a test condition of $M=0.8$, $Q=128$ psf. It is seen that the response has significant energy throughout the frequency range with particularly pronounced response in the neighborhoods of 150 and 500 Hz.

Compensation for Phase Lag

The use of digital control necessarily introduces delays in the command to the actuator that results from the accelerometer responses. These delays result from the computation time required of the digital computer and from the fact that analog-to-digital converters sample serially and not continuously. This delay translates into a phase lag in the command to the controller relative to a command that would emanate from a comparable analog control law. An even more pronounced source of phase lag is from the antialiasing filters discussed in the previous subsection.

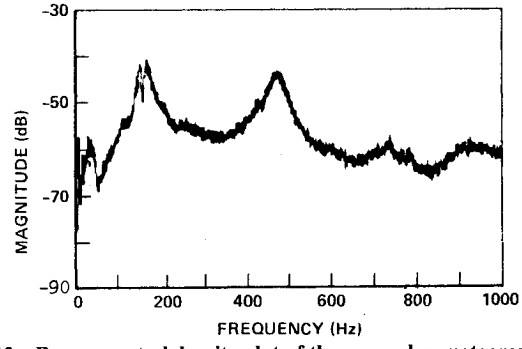

Fig. 12 Power spectral density plot of the a_4 accelerometer response, digital control law N3, $Q=128$ psf, $M=0.8$.

At the test site, a procedure was adopted whereby the phase difference between the analog and digital controllers was measured prior to a test run. A digital representation of a phase lead circuit was then introduced to compensate for the lag. The phase lead was accomplished using a digital representation of a first-order analog circuit that has a transfer function of the form

$$H=(\tau s-1)/(\tau s+1) \tag{9}$$

The value of τ was determined based on the amount of phase lead required at 6 Hz. Values of phase lead varied 12-25 deg, depending on the time frame and the antialiasing filters in place. A drawback of the first-order implementation is that the phase is correct at only one frequency, but this did not appear to have affected the system performance.

Conclusions

The transition from analog to digital control for wing/store flutter suppression can be characterized as being a demanding

but straightforward exercise. As discussed previously in this paper, factors related to aliasing and computational phase lags were the primary difficulties that had to be addressed to achieve a successful wind-tunnel demonstration. Aliasing was addressed by the implementation of high-order low-pass filters, while a simple first-order system was implemented to account for phase lags introduced by the discrete sampling of the digital control system.

It should be stressed that the fact the digital control laws did not perform as well as the comparable analog laws should not be construed to mean that they could not do so. It is believed that a control systems designer, experienced in methods of digital design, could use the power and flexibility of the digital computer to improve on the results presented in this paper.

The results of the preceding section provide ample evidence that the digital control of unstable, moderately high-frequency structures is feasible. This provides the control system designer with greatly increased flexibility. In particular, it paves the way for the demonstration of adaptive control, which requires the complex logic that is readily mechanized only on a digital system. In a more general sense, this demonstration shows that a flutter suppression system can be made compatible with the digital control systems that are becoming the norm in advanced aircraft.

Acknowledgments

The work reported in this paper was conducted under AFWAL Contract F33615-80-C-3217, Test Demonstration of Digital Adaptive Control of Wing/Store Flutter. The Air Force project engineer was Larry J. Huttsell. The test engineer at the NASA Langley Research Center's Transonic Dynamics Tunnel was Moses G. Farmer.

Other than the authors, key participants from Northrop included George R. Mills, Don L. Patton, and James R. Evans.

References

[1] Hwang, C., Johnson, E.H., Mills, G.R., and Pi, W.S., "Additional Demonstration of Active Wing/Store Flutter Suppression Systems," AFWAL-TR-80-3093, Aug. 1980.

[2] *Report on a Cooperative Programme on Active Flutter Suppression,* AGARD Conference Proceedings, Rept. 689, Aug. 1980.

[3] Hwang, C., Johnson, E.H., and Pi, W.S., "Recent Development of the YF-17 Active Flutter Suppression System," *Journal of Aircraft,* Vol. 18, July 1981, pp. 537-545.

[4] Harvey, C.A., Johnson, T.L., and Stein, G., "Adaptive Control of Wing/Store Flutter," AFFDL-TR-79-3091, April 1979.

[5] Edwards, J.W., "Flight Test Results of an Active Flutter Suppression System Installed on a Remotely Piloted Research Vehicle," *Proceedings of the AIAA/ASME/ASCE/AHS 22nd Structures, Structural Dynamics and Materials Conference,* Pt. 2, Atlanta, Ga., April 1981, p. 778-789.

[6] Peloubet, R.P. Jr., Haller, R.L., and Bolding, R.M., "F-16 Flutter Suppression System Investigation and Wind Tunnel Tests," *Journal of Aircraft,* Vol. 19, Feb. 1982, pp. 169-175.

[7] Mathew, J.R., "Developing, Mechanizing and Testing of a Digital Active Flutter Suppression System for a Modified B-52 Wind Tunnel Model," NASA CR 159155, March 1980.

[8] Hwang, C. and Pi, W.S., "Application of Optimal Control Techniques to Aircraft Flutter Suppression and Load Alleviation," *Proceedings of the AIAA/ASME/ASCE/AHS 23rd Structures, Structural Dynamics and Materials Conference, Pt. 2,* New Orleans, La., May 1982, pp. 427-438.